ACS Sustainable Chemistry & Engineering

pubs.acs.org/journal/ascecg

Research Article

Effect of Interstage Hydrothermal Treatment on Anaerobic Digestion of Sewage Sludge: Speciation Evolution of Phosphorus, Iron, and Sulfur

Qian Wang, Chiqian Zhang, Pan Liu, Haesung Jung, Biao Wan, Dhara Patel, Spyros G. Pavlostathis, and Yuanzhi Tang*

Cite This: *ACS Sustainable Chem. Eng.* 2020, 8, 16515−16525

Read Online

ACCESS | Metrics & More | Article Recommendations | Supporting Information

ABSTRACT: Anaerobic digestion (AD) with interstage hydrothermal treatment (HT) (i.e., AD−HT−AD) is an emerging technology for energy and nutrient recovery from sewage sludge. Yet, systematic understanding on the speciation evolution of nutrient phosphorus (P) and other redox-sensitive elements iron (Fe) and sulfur (S) during AD−HT−AD is still missing. This study investigated the coupled changes of P, Fe, and S speciation during AD−HT−AD of sewage sludge using complementary chemical extraction, microscopy, and spectroscopy analyses. Results indicated that after the first-stage AD a significant fraction of Fe was present as vivianite in the AD solids due to the microbial reduction of strengite and other Fe(III) species. During HT of the anaerobically digested solids, less vivianite but more strengite formed in the HT hydrochars with increasing HT temperature. Partial auto-oxidation of vivianite by H_2O at high HT temperatures (155 and 185 °C) induced the formation of strengite. For the second-stage AD, more vivianite formed in AD solids as compared to that in their corresponding hydrochars from higher HT temperatures (155 and 185 °C). Regarding S speciation, both AD stages and HT favored the formation of iron sulfides. Results from this study suggest that the cycling of both P and S is strongly coupled with Fe chemistry. This study sheds light on the reaction mechanisms during AD−HT−AD of sewage sludge and the nutrient recycling and reclamation options for sewage sludge management.

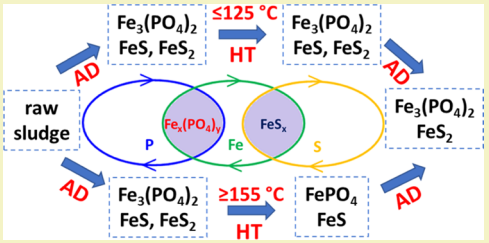

KEYWORDS: *anaerobic digestion, interstage hydrothermal treatment, vivianite, Fe sulfides, X-ray absorption spectroscopy*

INTRODUCTION

Municipal wastewater treatment facilities generate millions of tons of sewage sludge annually in the United States,[1] with the residue biowaste (biosolids) as a byproduct of wastewater treatment.[2] Sewage sludge intrinsically has a high water content[3] and contains various contaminants such as organics, heavy metals, and pathogens.[4] These properties of sewage sludge require environmentally positive management strategies before its final disposal or application. On the other hand, substantial amounts of nutrients (such as phosphorus, P, and nitrogen, N) and energy elements (such as carbon, C) consumed by human activities converge into sewage sludge, making it a candidate source for resource recovery.[4−6] For instance, energy recovery can be achieved through the production of biomethane during anaerobic digestion (AD) of sewage sludge.[7] P recycling/reclamation from sewage sludge is also a promising strategy to address the societal concerns related to the depletion of geological P sources.[8,9]

AD degrades complex organic matter (OM) in sewage sludge and produces biomethane through four distinct subprocesses (hydrolysis, acidogenesis, acetogenesis, and methanogenesis).[10] AD is also a core biotechnology for the recovery of nutrients such as P and N. During AD, sewage sludge releases soluble phosphate and NH_4^+ to the liquid phase, which can be recovered via struvite ($MgNH_4PO_4 \cdot 6H_2O$) precipitation.[11] In addition, as iron (Fe) salts are common flocculants in municipal wastewater treatment, Fe is one of the most abundant metal ions in sewage sludge.[4] Therefore, Fe phosphate mineral vivianite ($Fe_2(PO_4)_3 \cdot 8H_2O$) is the main phosphate source in some anaerobically digested sludge.[12−16]

Although the AD of sewage sludge has advantages on energy recovery, the conversion rate of OM to biogas (biomethane and CO_2) is limited because of the recalcitrant nature of particulate OM.[17] The rate-limiting step of AD is the hydrolysis,[18] which involves the conversion of particulate polymeric OM into bioavailable substrates for acidogenesis and acetogenesis.[10] To accelerate hydrolysis, researchers have extensively explored various thermal, chemical, mechanical,

Received: July 29, 2020
Revised: October 12, 2020
Published: October 29, 2020

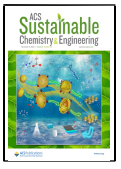

and biological methods.[19] AD coupled with pre- or interstage hydrothermal treatment (HT) (i.e., sequential HT−AD or AD−HT−AD, respectively) is effective in accelerating hydrolysis and improving the biodegradability of particulate OM. Both HT−AD and AD−HT−AD were shown to significantly enhance biogas production,[20−22] facilitate sludge dewatering and volume reduction, as well as sanitize biosolids and improve their quality as soil amendments.[23,24] Several studies have demonstrated that AD−HT−AD performs better than HT−AD with respect to methane production, energetic benefit of the whole treatment, volatile solid destruction, and greenhouse gas emission.[20,21,25] In addition, AD−HT−AD offers another advantage of achieving Class A biosolids.[25] Our recent study investigated the speciation evolution of C and P in sewage sludge and manure during the sequential HT−AD process.[26] However, systematic understanding on the evolution of nutrients during sequential AD−HT−AD is still lacking. In the United States, ∼60% of sewage sludge is land-applied;[27,28] thus, studies on the transformation of P speciation during sequential AD−HT−AD will greatly enhance our understanding on the recycling and utilization options of P from the treated sewage sludge.

Fe and sulfur (S) are two abundant redox-sensitive elements in sewage sludge.[9] Our recent study revealed the strong correlations between Fe and P species and Fe and S species during the sequential HT−AD process. For a mixture of primary and waste activated sludge, hydrothermal pretreatment at high temperatures (155 and 185 °C) inhibited vivianite formation and imposed weak effects on the sulfidation of Fe during the subsequent AD.[29] Compared with primary and waste activated sludges, vivianite and Fe sulfides are the major Fe species in anaerobically digested sludge without hydrothermal pretreatment.[12,16] Vivianite can be recovered through magnetic separation.[30] However, the effects of interstage HT on the evolution of vivianite in sewage sludge during AD−HT−AD remain unclear. As to Fe sulfides, they can control the mobility and bioavailability of toxic metals (e.g., Hg(II), Cu(II), and Pb(II)) and metalloids (e.g., arsenite) through sorption.[31−33] Given that the presence of Fe sulfides in sludge can affect the performance of sludge land application, it is thus important to understand the evolution of Fe sulfides in sewage sludge during AD−HT−AD. In addition, from the perspective of treatment product utilization, a systematic comparison of AD−HT−AD, HT−AD, and AD is still missing.

This study investigates the potential coupling or coevolution of P, Fe, and S speciation in sewage sludge during sequential AD−HT−AD, which is expected to provide insights into the chemical environment in operation and P recovery from sewage sludge. HT temperature dictates the thermal hydrolysis process, and HT below 190 °C was previously shown to increase biomethane yield during the subsequent AD.[34] Thus, we conducted HT at four representative temperatures (90, 125, 155, and 185 °C) to assess the effect of HT temperature on sludge hydrolysis. The raw sewage sludge, solids from both AD stages, and HT hydrochars were characterized using complementary chemical extraction, X-ray absorption spectroscopy (XAS), X-ray diffraction (XRD), and scanning electron microscopy with energy-dispersive X-ray spectroscopy (SEM-EDXS).

MATERIALS AND METHODS

Experimental Setups. Sewage sludge samples were obtained from the F. Wayne Hill Water Resources Center, a municipal wastewater treatment facility in Buford, GA. The center uses primary (physical), secondary (biological), and anaerobic digestion treatment units, as well as a waste activated sludge stripping unit for the storage of sludge mixture and P removal. The center uses enhanced biological phosphorus removal (EBPR) and does not dose any Fe for phosphorus removal. Sludge mixture, secondary effluent, and digestate from the plant anaerobic digester were collected and stored in the dark at 4 °C prior to use. The sludge mixture was the blend of primary and waste activated sludges, with a total solid (TS) mass ratio of 63/37 and a TS concentration of ca. 60 g/L. The Fe/P molar ratio in the sludge mixture was 0.27 (Table S1). The sludge mixture was chosen for the experiments, as primary and waste activated sludges are mixed and then fed to the onsite AD in most water resource recovery facilities (WRRFs). The digestate was anaerobically incubated at 35 °C in the lab until no significant biogas production and served as the anaerobic inoculum.

During AD−HT−AD, the first-stage AD was conducted in a capped 9 L anaerobic glass reactor stirred with a magnetic stirring bar (∼220 rpm) at 35 °C for 15 days. For the interstage HT, 15-day digested slurries were loaded to polypropylene-lined stainless steel hydrothermal reactors (COL-INT TECH., SC, USA). Each hydrothermal reactor (200 mL) contained 130 mL slurries. The reactors were tightly sealed and heated in an oven at 90, 125, 155, or 185 °C for 4 h (3 h ramping and 1 h holding time at the target temperature) and cooled down to room temperature naturally. The second-stage AD was conducted in capped 600 mL glass reactors mixed using an orbital shaker (∼220 rpm) at 35 °C for 74 days. The detailed composition of suspensions in the first- and second-stage anaerobic reactors is given in Table S2. The 15-day digested slurries without HT were anaerobically incubated using the same procedures as the control experiment. No medium was used during all AD experiments. For both AD stages, the total biogas volume and composition were monitored periodically, which will be published in a parallel study.

At the end of each AD, a portion of AD slurries was immediately transferred to a COY anaerobic chamber (95% N_2/5% H_2; COY Lab), preventing exposure to air that can induce the oxidation of the redox-sensitive Fe and S. The solids (hereinafter referred to as AD solids) and liquid (hereinafter referred to as AD process water) were separated using 0.45 μm membrane filters. The obtained AD solids were air-dried and stored in the anaerobic chamber. For HT, a portion of HT slurries was centrifuged to separate the solids (hereinafter referred to as hydrochars, although HT at 90 and 125 °C does not readily converts biomass to chars) and liquid (hereinafter referred to as HT process water). The HT hydrochars were freeze-dried until no further weight loss. The same procedure was also performed for the raw sludge mixture slurries. All of the dried solid samples were finely ground and stored in the anaerobic chamber prior to characterization (details below). The concentrations of major metals in the dried raw sludge mixture are given in Table S1. Sample labels and treatment conditions are described in Table 1.

Analytical Methods. Aqua regia digested solid samples and process water samples were analyzed by inductively coupled plasma optical emission spectrometry (ICP-OES) for total P, Fe, and S concentrations. Solid samples were analyzed by XRD and SEM-EDX. P, Fe, and S speciation were characterized by sequential chemical extraction (SCE), P and S K-edge X-ray absorption near-edge structure (XANES) spectroscopy, and Fe K-edge extended X-ray absorption fine structure (EXAFS) spectroscopy, as detailed in Text S1, Supporting Information (SI).

For P XANES spectra, principal component analysis (PCA) and target transformation (TT) were performed on the spectra to determine the number of member components and identify candidate P species for the subsequent linear combination fitting (LCF) analysis. LCF analysis of the P K-edge XANES spectra was conducted at an energy range of −20 to +60 eV relative to the edge energy to quantify the P species in the solid samples. Goodness of the fit was evaluated using the residual factor (R-factor), and the fits with the smallest R-factors were deemed good. A set of P reference compounds were used for LCF analysis, including (1) strengite ($FePO_4{\cdot}2H_2O$), phosphate-adsorbed ferrihydrite (P-Ferrihy), and vivianite, represent-

https://dx.doi.org/10.1021/acssuschemeng.0c05544
ACS Sustainable Chem. Eng. 2020, 8, 16515−16525

Table 1. Sample Labels and Reaction Conditions of Hydrothermal Treatment (HT) and Anaerobic Digestion (AD) Processes[a]

sample label	treatment	reaction condition
SWE		secondary wastewater effluent, pH 7.26
AI		anaerobic inoculum, pH 8.14
AAI	AD	AD of AI till no biogas production, 35 °C, pH 7.96
raw sludge	-	raw sludge, pH 6.34
A15	AD	AD of raw sludge, 35 °C, 15 days, pH 7.60
A89	AD−AD	AD of A15 slurries, 35 °C, 74 days (89 days AD in total), pH 8.44
AH90	AD−HT	HT treatment of A15 slurries, 90 °C, 4 h, pH 7.53
AH90A	AD−HT−AD	AD of AH90-derived slurries, 35 °C, 74 days, pH 8.45
AH125	AD−HT	HT treatment of A15 slurries, 125 °C, 4 h, pH 7.26
AH125A	AD−HT−AD	AD of AH125-derived slurries, 35 °C, 74 days, pH 8.38
AH155	AD−HT	HT treatment of A15 slurries, 155 °C, 4 h, pH 7.24
AH155A	AD−HT−AD	AD of AH155-derived slurries, 35 °C, 74 days, pH 8.37
AH185	AD−HT	HT treatment of A15 slurries, 185 °C, 4 h, pH 6.91
AH185A	AD−HT−AD	AD of AH185-derived slurries, 35 °C, 74 days, pH 8.23

[a]pH values were measured after HT/AD treatments.

ing Fe-associated P; (2) $AlPO_4$ and phosphate-adsorbed γ-alumina (P-alumina), representing Al-associated P; (3) octacalcium phosphate (OctaCa) and hydroxylapatite (HydAp), representing Ca-associated P; and (4) phytic acid (PhyAc), representing organic phosphate. Details on these reference compounds are in Table S3.

LCF analysis of Fe EXAFS data was conducted in the k^3-weighted χ-space (3−11.5 $Å^{-1}$) using a library of Fe reference compounds (Table S3), including two-line ferrihydrite (Ferrihy), goethite, hematite, lepidocrocite, magnetite, siderite, carbonated green rust (CGR), sulfated green rust (SGR), vivianite,[35] strengite,[36,37] and Fe(III)-organic complex (Fe(III)-OM).[38] LCF analysis of the S XANES data used a group of S reference compounds, including FeS, FeS_2,[39] cystine,[40] cysteine,[41] methionine methylsulfonium chloride, methionine sulfoxide, methionine sulfone, anthraquinone sulfonic acid,[40] chondroitine sulfate,[42] and $CaSO_4$ (Table S3). Spectra of the P, Fe, and S reference compounds are provided in Figure S1.

RESULTS AND DISCUSSION

Speciation of P, Fe, and S during the First-Stage AD.

The first-stage AD of raw sludge increased the total P concentration in the AD solids and released P into process water, as can be seen for the raw sludge and A15 samples in Table S4. After the first-stage AD, the total P concentration increased from 1.92% (raw sludge) to 3.42% (sample A15). The increase was due to the decomposition of OM and biogas production[13] and the introduction of P from the anaerobic inoculum (Table S4). P concentration in the process water also increased from 0.19 mM (raw sludge) to 0.25 mM (sample A15), suggesting P release from the solids during AD. Previous studies also showed that AD process favors P release.[43] The possible causes of P release from the solids were dissolution of metal-phosphate precipitates and degradation of organic P by anaerobic microbes,[44] as well as hydrolysis of phosphate-accumulating organisms (PAOs).[45]

AD process also affected P speciation in the solids, as revealed by P XANES data (Figure S2) and LCF analyses (Table 2 and Figure S3). LCF analyses identified strengite (23.0%), $AlPO_4$ (32.5%), P-alumina (14.5%), HydAp (9.2%), and PhyAc (16.0%) as the main P species in raw sludge (Table 2). Organic P species were absent in sample A15, consistent with the SCE results showing the predominance of inorganic P in this sample (Text S2). The fractions of strengite, $AlPO_4$, and HydAp decreased in sample A15 as compared to those of raw sludge. However, the fractions of vivianite, P-alumina, and OctaCa increased from 0, 14.5, and 4.8% in raw sludge to 37.8, 22.6, and 13.4% in sample A15, respectively (Table 2).

As P transformation is strongly coupled with Fe, we discuss Fe chemistry below. The total Fe concentration in the solids increased from 0.93% (raw sludge) to 3.49% (sample A15) after the first-stage of AD (Table S4). As can be seen from Fe XANES and EXAFS spectra of A15 solids, both the main edge and pre-edge peak positions shifted to lower energy as compared to raw sludge (Figure S5), suggesting the reduction of Fe(III) to Fe(II) during AD. The k^3-weighted Fe EXAFS spectra of raw sludge had four characteristic oscillations at 4.2, 6.5, 8.5, and 10.0 $Å^{-1}$ (Figure 1a). For A15 solids, the oscillations at 5.1 and 7.5 $Å^{-1}$ occurred. Meanwhile, the left shifting of the oscillations at 4.2 and 6.5 $Å^{-1}$ and the flattened oscillations at 8.5 and 10.0 $Å^{-1}$ were observed (Figure 1a).

Table 2. Relative Abundance of Different P Species Determined from Linear Combination Fitting (LCF) of P K-Edge XANES Data of the Solid Samples[a]

	relative abundance (%)								
	Fe-associated P			Al-associated P		Ca-associated P			
sample	vivianite	strengite	P-ferrihy	$AlPO_4$	P-alumina	HydAp	OctaCa	PhyAc	*R*-factor
raw sludge		23.0 (2.7)		32.5 (0.9)	14.5 (1.9)	9.2 (1.7)	4.8 (3.7)	16.0 (2.8)	0.0007
A15	37.8 (1.4)	17.4 (2.1)		8.8 (0.3)	22.6 (0.8)		13.4 (0.6)		0.0003
A89	58.5 (3.9)	8.4 (5.9)		9.1 (2.8)	5.3 (2.9)		18.7 (1.5)		0.0026
AH90	44.7 (1.6)	9.2 (3.2)	7.4 (1.6)		32.5 (1.8)		6.2 (0.8)		0.0005
AH90A	43.4 (0.6)	5.9 (1.2)		5.7 (0.8)	32.0 (0.7)	3.9 (0.1)	9.1 (0.3)		0.0001
AH125	43.4 (2.1)	7.4 (4.2)	4.5 (2.1)	17.6 (2.7)	8.9 (2.3)		18.2 (1.1)		0.0021
AH125A	40.5 (1.0)	8.3 (1.7)		6.7 (1.1)	27.3 (1.0)	2.2 (0.2)	15.0 (0.4)		0.0002
AH155	18.3 (3.8)	36.6 (5.8)			23.8 (3.1)		21.3 (1.5)		0.0016
AH155A	39.4 (1.2)	8.5 (2.7)			39.4 (1.6)	2.3 (0.3)	10.4 (0.7)		0.0004
AH185	2.9 (8.3)	41.6 (12.7)		11.4 (4.8)	23.0 (6.8)	2.7 (3.8)	18.4 (3.3)		0.0039
AH185A	25.2 (0.7)	15.7 (2.0)		19.3 (1.3)	28.4 (1.3)	2.4 (0.2)	9.0 (0.8)		0.0002

[a]Note: LCF analysis-derived errors are given in parentheses.

https://dx.doi.org/10.1021/acssuschemeng.0c05544
ACS Sustainable Chem. Eng. 2020, 8, 16515−16525

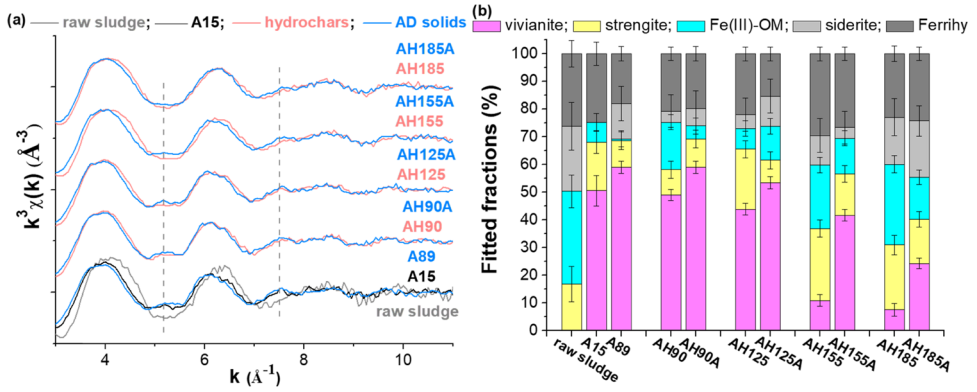

Figure 1. (a) Fe k^3-weighted EXAFS spectra of the raw sludge, HT hydrochars, and AD solids, as well as (b) their corresponding Fe speciation quantified by LCF analysis. Fe(III)-organic complex (Fe(III)-OM) and ferrihydrite (Ferrihy).

These characteristic features are for vivianite,[36,46] suggesting that vivianite was the predominant Fe species in A15 solids.

To quantify Fe speciation in A15 solids, LCF analyses of Fe EXAFS spectra were performed using a range of representative Fe reference compounds. Best fits were obtained with five compounds: strengite, vivianite, Ferrihy, CGR, and Fe(III)-OM (Table S5 and Figure S6). Strengite (20%), Ferrihy (22%), Fe(III)-OM (30%), and CGR (20%) were identified as the main Fe species in raw sludge, whereas vivianite (42%), strengite (10%), Ferrihy (5%), Fe(III)-OM (5%), and CGR (20%) were the main Fe species in A15 solids (Table S5 and Figure S6), suggesting the accumulation of vivianite in A15 solids. XRD analysis also confirmed the presence of vivianite in A15 solids (Figure 2). The inclusion of CGR as a reference compound for LCF analysis yielded the best fit (i.e., the smallest *R*-factor). Considering that CGR is unstable, we also conducted LCF by replacing CGR with siderite, a more stable and common compound in sewage sludge.[30,47] With this reference compound combination, the fitting results (Table S6 and Figures 1b and S7) showed 24% siderite in raw sludge and no siderite after AD. We also observed a similar trend for the changes for vivianite, strengite, Fe(III)-OM, and Ferrihy between raw sludge and A15 solids (Figure 1b). Note that both CGR and siderite are Fe(II)-containing species; replacing one by the other did not affect the overall trend in Fe speciation evolution. The small difference in fitted fractions was likely caused by the intrinsic limitation of LCF analysis with an error range of <10%.

Mineral particles with high contents of both Fe and P in A15 solids were analyzed by SEM-EDX (Figure S8 and Table S7). In addition to a certain amount of Si and S in some particles, Ca, Al, and Mg coexisted at relatively high concentrations with the Fe phosphate minerals (Table S7). Impurity inclusion of Fe phosphate minerals is common, as other cations can replace Fe atoms in Fe phosphate mineral structures.[48−50] Previous studies also showed that vivianite is not present as free particles in anaerobically digested sludges.[13,51]

Considering the commonly observed strong coupling between Fe and S chemistry in anaerobically digested sludges,[16,52] we discuss S chemistry below. The total S concentration in A15 solids increased from 0.72% (raw sludge) to 1.11% (sample A15) after the first-stage AD, whereas the change in S concentration in process waters was minimal (Table S4). The S K-edge XANES spectra of raw sludge had oscillations at 2472.6, 2473.2, 2481.0, and 2482.5 eV (Figure 3), representing zero-valent S, thiols (+0.5), sulfonates (+5), and sulfates (+6),[41] respectively. Compared with raw sludge, the main difference observed for A15 solids was the left shifting of the peak at 2474 eV. In addition, the oscillation intensities of S (+5 and +6) at 2481.0 and 2482.5 eV decreased slightly (Figure 3a), suggesting the reduction of S. The reference compounds used for LCF analysis included FeS, pyrite, S (0), thiols (+0.5), sulfonates (+5), and sulfates (+6). Given that S K-edge XANES spectra are more sensitive to different oxidation states of S compounds,[41,53] the S reference compounds used in this study do not refer to the exact compound structures. The fitting results are shown in Table S8 and Figures 3b and S9. For raw sludge, the main S species were S (0) (∼15%), S (+0.5) (∼52%), S (+5) (∼6%), and S (+6) (∼20%). After the first-stage AD, the fractions of S (0), S (+0.5), and S (+6) did not change significantly, but the fraction of S (+0.5) decreased from 55 to 38% with the occurrence of both FeS and pyrite (14% in total). The formation of Fe sulfides was due to the microbial reduction of Fe(III) species and organic S during AD.[16,54] Pyrite is a very crystalline component, but XRD did not confirm its presence (Figure 2a). That is because the content of pyrite in A15 solids (i.e., ∼0.11%) was below the detection limit of XRD (∼3%).

Taken together, the mechanisms of the linked evolution of P, Fe, and S during the first-stage AD are illustrated in Figure 4. Biotic reduction of Fe(III) species such as strengite, Fe(III)-OM, and Fe(III) oxides led to the production of Fe(II).[3,55] The reductive dissolution of strengite[56] and degradation of organic P generated soluble phosphate,[57] which precipitated with Fe(II) to form vivianite. Approximately 15% of the S species existed as Fe sulfides as indicated by LCF analysis of S XANES data. However, LCF analysis of Fe EXAFS data did not identify the predominant contribution from Fe sulfide phases, likely due to the much higher total concentration of Fe than of S in the AD solids (Table S4). The content of Fe sulfides in A15 solids was not as high as previous studies dosing Fe to anaerobic digestors for the formation of Fe sulfides,[16] as EBPR is employed in F. Wayne Hill Water Resources Center resulting in a high molar ratio of P:Fe but a low molar ratio of S:Fe in raw sludge (Table S4). In addition, pyritization is considered to be a slow process in anaerobic digesters,[58] while phosphate precipitates preferentially with Fe(II) as vivianite.[13] Overall, the reducing environment during AD favored the precipitation of vivianite and Fe sulfides in the AD solids.

Speciation of P, Fe, and S during HT. HT strongly affected the total concentrations of P and Fe in the hydrochars.

https://dx.doi.org/10.1021/acssuschemeng.0c05544
ACS Sustainable Chem. Eng. 2020, 8, 16515−16525

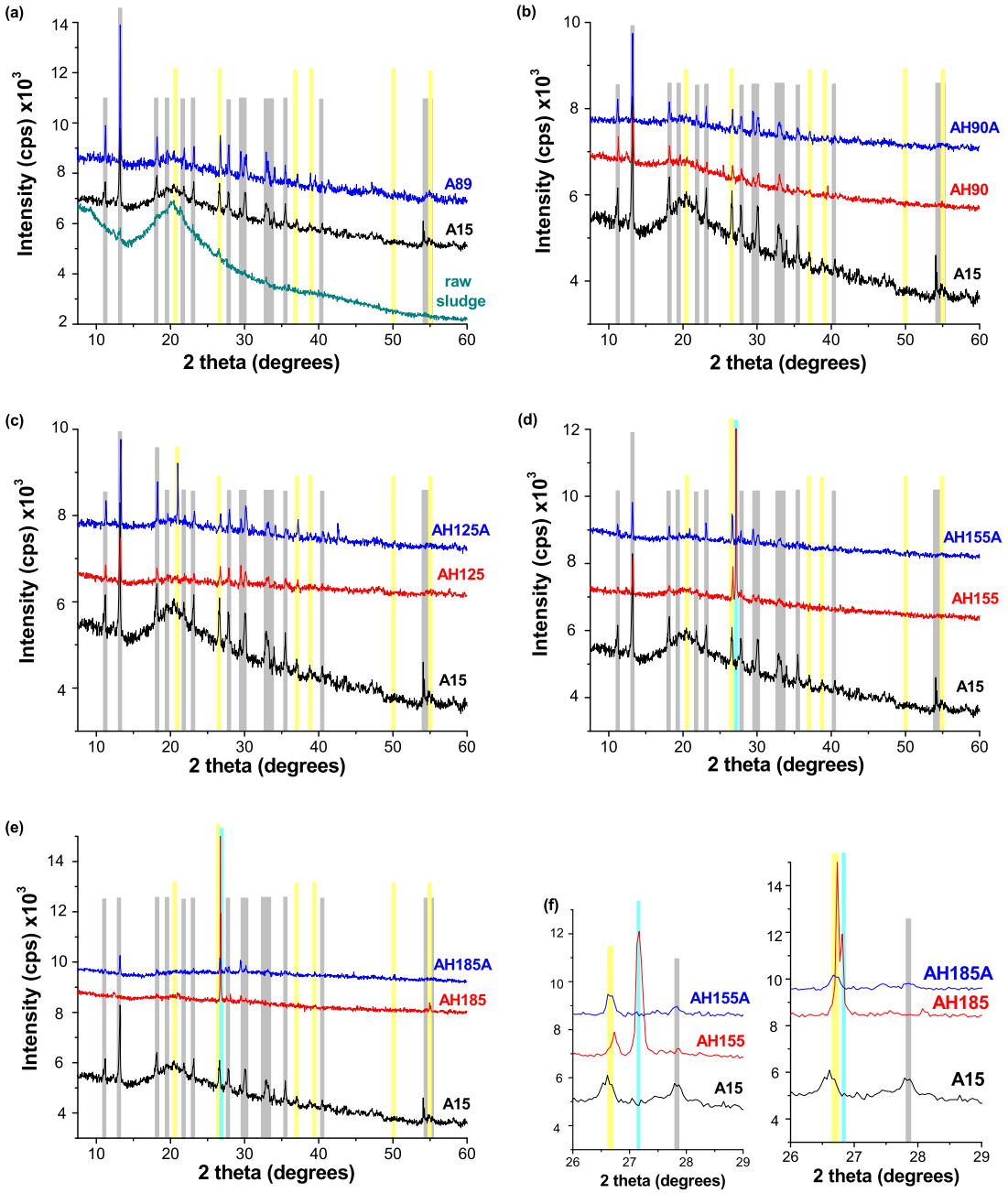

Figure 2. (a-e) XRD patterns of the raw sludge, HT hydrochars, and AD solids. Panel (f) is a zoomed view of the XRD patterns at 26−29° 2θ of panels (d) and (e). In each panel, the gray, yellow, and cyan vertical bars indicate XRD peak positions of vivianite (PDF #83-2453), quartz (PDF #46-1045), strengite (PDF #03-0379), and strengite (quartz-like phase, PDF #17-0837), respectively.

Compared with sample A15, the total concentrations of both P and Fe in the hydrochars increased with increasing HT temperature (Table S4). For sample AH185, P and Fe concentrations were 5.90 and 6.36%, respectively. The accumulation of P and Fe in hydrochars was due to the decomposition of OM.[59,60] The total P concentration in process waters remained at 0.25 mM for sample AH90, but slightly increased to ∼0.36 mM for samples AH125, AH155, and AH185. A little higher concentration of P in HT process waters than sample A15 was probably due to release of P from P-associated OM during decomposition of OM by HT. The concentration of Fe in process waters was low (7.3−18.4 μM), consistent with previous observations that HT concentrated heavy metals in hydrochars.[59] Compared with sample A15, the changes in the total S concentration in HT hydrochars were subtle (Table S4), probably because the loss of OM was in proportion to the release to organic S during HT. Accordingly, the elevated S concentration in process waters was observed. It was due to the decomposition of organic S and the release of S species into process waters.[61]

HT significantly changed P, Fe, and S speciation in hydrochars. P speciation in hydrochars was identified by the LCF analysis of P XANES spectra (Table 2 and Figures S2 and S3). Compared with A15 solids, the changes in the fraction of P species in samples AH90 and AH125 were within 10% (Table 2). This suggests that the main P species did not change significantly at low HT temperatures by considering the uncertainty in fitting (typical error range of ∼10% for LCF).

https://dx.doi.org/10.1021/acssuschemeng.0c05544
ACS Sustainable Chem. Eng. 2020, 8, 16515−16525

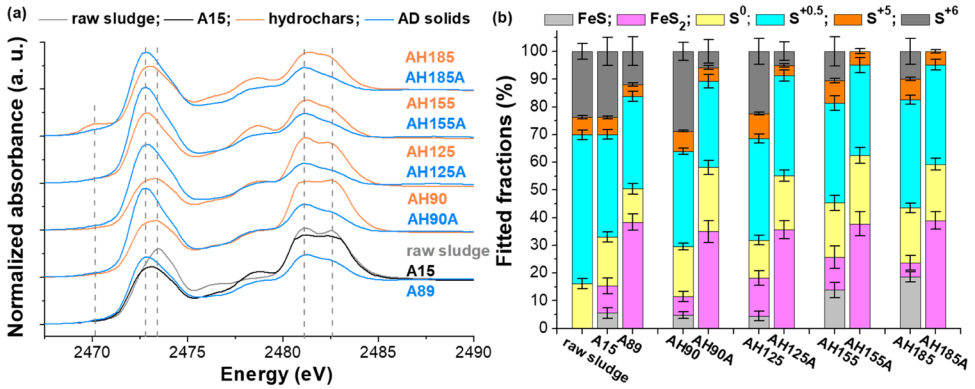

Figure 3. S K-edge XANES spectra (a) of the raw sludge, HT hydrochars, and AD solids, and their corresponding S speciation (b) quantified by LCF analysis.

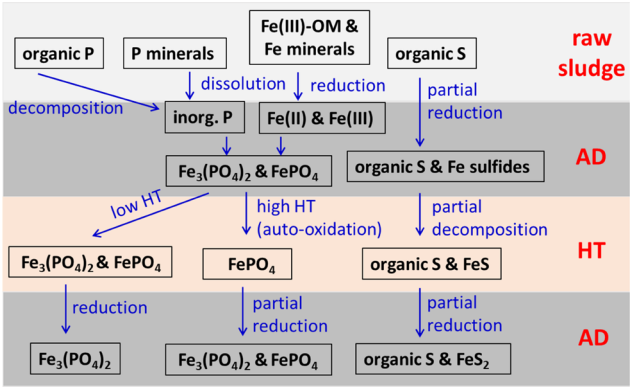

Figure 4. Proposed reaction mechanisms for the coevolution of P, Fe, and S speciation in sewage sludge during anaerobic digestion with interstage hydrothermal treatment (AD−HT−AD).

However, the fraction of strengite in hydrochars increased from 17.4% (sample A15) to 36.6% (sample AH155) and 41.6% (sample AH185), whereas vivianite fraction decreased from 37.8% (sample A15) to 18.3% (sample AH155) and 2.9% (sample AH185) (Table 2). These data suggest that a large amount of vivianite was transformed to strengite at high HT temperatures (155 and 185 °C). Generally, the fraction changes of Ca- and Al-associated P species in hydrochars as compared to those of sample A15 were within 10% (Table 2). SEM-EDX suggests that P species were not uniformly distributed in hydrochars (e.g., AH155), and iron phosphate minerals were enriched in sample AH155 in close association with Ca and Al phosphate minerals (Figure S8 and Table S7).

Compared with sample A15, the Fe XANES and EXAFS spectra of sample AH90 were similar (Figures S5 and 1b). However, a right shifting of the white-line peak and pre-edge peak was observed for samples AH125, AH155, and AH185 as compared to that for sample A15, suggesting the oxidation of Fe(II) to Fe(III) during HT. Higher HT temperatures (155 and 185 °C) led to more significant peak shifting (Figures S5 and 1b). Fe EXAFS spectra of HT hydrochars showed that the intensities of oscillations at 5.1 and 7.5 $Å^{-1}$ decreased and the oscillation at 4.2 $Å^{-1}$ right-shifted for AH125 as compared to that for sample A15. These feature changes became stronger with increasing HT temperature (Figure 1a). LCF-quantified Fe species in the hydrochars are given in Tables S5 and S6 and Figures 1b and S6b. Similar LCF results were obtained using two sets of reference compounds including CGR or siderite as previously discussed. With increasing HT temperature, the fraction of ferrihydrite in HT hydrochars did not change, vivianite decreased, and strengite and Fe(III)-OM increased in fractions. For instance, sample AH90 contained vivianite, strengite, and Fe(III)-OM at ∼38, ∼6, and ∼16%, respectively. However, the fractions of the above species for sample AH185 were <5, ∼21, and ∼28%, respectively. In general, the changes of vivianite and strengite fractions derived from Fe EXAFS LCF analysis were consistent with P XANES LCF analysis. XRD analysis confirmed the appearance of a small amount of vivianite in HT hydrochars. Strengite also appeared in samples AH155 and AH185 (Figure 2), as evidenced by the presence of the diffraction peak at ∼27°.[62] It is the main diffraction peak of strengite, which can shift slightly after heating.[62]

Compared with the S XANES spectra of sample A15 (Figure 3a), the intensity of sulfate (+6) oscillation for hydrochars decreased with increasing HT temperature. Meanwhile, the oscillation at 2473.2 eV slightly shifted to the right. Moreover, the pre-edge feature at 2470 eV was pronounced for sample AH185. Based on S XANES LCF, HT did not change the fractions of FeS_2, zero-valent S, cysteine (+0.5), and sulfonate (+5). However, with increasing HT temperature, the fraction of sulfate (+6) decreased, while the FeS fraction increased. For sample AH185, the sulfate fraction was ∼8%, while the FeS fraction was 17%. The high FeS content accounted for the occurrence of the pronounced pre-edge feature at 2470 eV.

Taken together, the transformation pathways of P, Fe, and S during the interstage HT are given in Figure 4. Vivianite remained as the predominant species for both Fe and P in low-temperature HT hydrochars (i.e., AH90 and AH125), but vivianite fraction did not change significantly as compared to sample A15. However, vivianite was partially transformed into strengite and other Fe(III) species at high HT temperatures (i.e., 155 and 185 °C). It was probably due to auto-oxidation of vivianite by decomposition of water during heating,[63−65] as described by the following equation

$$2\,Fe^{2+} + 2\,H_2O \rightarrow 2\,Fe^{3+} + 2\,OH^- + H_2 \quad (1)$$

Hanzel et al. also observed that (1) vivianite starts auto-oxidation at ∼100 °C for 5 h; (2) high temperature of heating favors the rate of auto-oxidation of vivianite; and (3) the auto-oxidation products, most probably strengite, inhibit further auto-oxidation process.[63] These reaction mechanisms can well explain our findings, i.e., partial oxidation of vivianite at 155 and 185 °C.

https://dx.doi.org/10.1021/acssuschemeng.0c05544
ACS Sustainable Chem. Eng. 2020, 8, 16515−16525

HT of sludge favors metal sulfidation and the precipitation of metal sulfide minerals.[59,66] Sulfide is generated by cracking the unstable mercaptan structure of organic S during HT.[67] In addition, up to 22% of S species as Fe sulfides were obtained from the S XANES LCF analysis, but Fe EXAFS LCF analysis did not fit out any Fe sulfides. That was because the total concentration of Fe in the HT hydrochars was 6.5 times higher than that of S (Table S4).

Speciation of P, Fe, and S during the Second-Stage AD. The second-stage AD further changed the elemental concentrations in AD solids and process waters. Compared with the first-stage AD of raw sludge, similar but stronger trends for the concentrations of P, Fe, and S in the solids and process waters were observed after the second-stage AD of sample A15 (Table S4). For instance, the total P concentrations in the solids and process waters of sample A89 were 3.71% and 0.62 mM, respectively, higher than those of sample A15. Compared with HT hydrochars, the total P concentration decreased in AD solids but increased in process waters after the second-stage AD. For sample AH185A, the total P concentrations in AD solids and process waters were 4.03% and 0.89 mM, respectively. Compared with A89, the total P concentrations in AD solids and process waters for AH185A increased. The high P concentration in the AD process waters was due to the release of P from the hydrochars, i.e., microbial dissolution of metal-phosphate precipitates. Fe concentration decreased in AD solids but remained low in process waters as compared to that of HT hydrochars. The decreased Fe concentration in the second-stage AD solids was due to the use of the anaerobic inoculum, which contained a lower Fe concentration than that of the HT hydrochars. Compared with the HT hydrochars, the total S concentration increased in the second-stage AD solids but decreased significantly in the process waters (Table S4). A previous study showed that sulfides were the dominant S species in AD process waters and preferably precipitated with metals.[68] In this study, no H_2S gas in the biogas was detected by gas chromatography analysis (data not shown) because most sulfides produced by microbial reduction existed in the suspensions at a high pH (pH 8).[54] Moreover, the absence of H_2S in the biogas was probably due to a high molar ratio of Fe:S in favor of the formation of Fe sulfides and the VS-based inoculum/substrate ratio (ISR) chosen in the present study (Table S2). Previous studies indicated that ISR could affect the biogas yield.[69]

The second-stage AD further affected P, Fe, and S speciation in the final AD solids. According to P XANES LCF analyses, the vivianite fraction increased from 37.8% (sample A15) to 58.5% (sample A89), while the fractions of strengite and P-Alumina decreased from 17.4 and 22.6% (sample A15) to 8.4 and 5.3% (sample A89), respectively (Table 2). These changes can be explained by the microbial reduction of strengite to dissolved Fe(II), which then precipitated with soluble phosphate. Wilfert et al. also reported that P existed predominantly as vivianite in AD sludge.[12] The fraction of vivianite in AH90A, AH125A, AH155A, and AH185A decreased as compared to that of sample A89, because their corresponding hydrochar samples contained higher fractions of Fe(III) species than sample A15. Compared with samples AH90 and AH125, the P speciation in samples AH90A and AH125A did not significantly change. However, for AH155A and AH185A solids, the fractions of strengite and OctaCa decreased compared with those of their corresponding hydrochars. Meanwhile, the vivianite fraction in samples AH155A and AH185A significantly increased (Table 2). For instance, the fractions of vivianite, strengite, and OctaCa in AH155A solids were 39.4, 8.5, and 18.4%, respectively (Table 2). Compared with sample AH155, the contents of Ca, Al, and Mg coexisting with Fe phosphate minerals in sample AH155A decreased (Figure S8 and Table S7), suggesting that the purity of Fe phosphate minerals in the final AD solids was higher. Fe phosphate minerals in the final AD solids could be purer, due to the higher concentration of soluble phosphate in the second-stage AD (Table S4).

We observed the left shifting of the white-line and pre-edge oscillations of Fe XANES spectra of sample A89 as compared to that of sample A15 (Figure S5), indicating the further reduction of Fe(III) during the second-stage AD. The Fe EXAFS spectra of A89 solids showed that the oscillations at 5.1 and 7.5 $Å^{-1}$ became more pronounced and the oscillations at 4.2 and 6.5 $Å^{-1}$ shifted to the left as compared to those of A15 solids (Figure 1a). These feature changes suggest that more vivianite formed in A89 solids. Compared with their corresponding HT hydrochars, the above changes of both Fe XANES and EXAFS spectra were also observed for AH90A, AH125A, AH155, and AH185A solids (Figures S5 and 1a). Furthermore, Fe EXAFS LCF analyses showed that the fractions of strengite, Ferrihy, and Fe(III)-OM in the final AD solids decreased, while the fraction of vivianite increased as compared to those of the corresponding HT hydrochars (Tables S5 and S6 and Figures 1b and S6b). For sample A89 solids, the fractions of vivianite and strengite reached ∼60 and 7%, respectively. For sample AH185A, the fractions of vivianite and strengite were 25 and 12%, respectively. In addition, the presence of CGR/siderite in the final AD solids (Tables S5 and S6 and Figures 1b and S6b) suggests that CO_2 was also involved in the Fe cycle during the second-stage AD. XRD confirmed the formation of vivianite after the second-stage AD (Figure 2).

Compared with sample A15 solids, the oscillation intensities of S (+5 and +6) from S XANES spectra significantly decreased for sample A89. In addition, the oscillation at 2473.2 eV shifted left and the oscillation at 2478 eV was much weaker for sample A89. These changes suggest the reduction of S with high oxidation state and the formation of sulfides. Similar trends were also observed for the final AD solids after the second-stage AD as compared to those of their corresponding HT hydrochars. According to S XANES LCF analyses, the changes were subtle for the fractions of S (0) and S (+0.5) in the final AD solids during the second-stage AD. The fractions of FeS, S (+5), and S (+6) in the final AD solids decreased significantly, while the fraction of pyrite increased to ∼37% as compared to those of HT hydrochars (Figure 3).

The formation of vivianite and pyrite was involved in the coevolution of P, Fe, and S in the second-stage AD (Figure 4). During the second-stage AD, biotic reduction of Fe(III) produced Fe(II), which was coupled with the oxidation of OM.[3,55] Biotic reduction of organic S generated much hydrogen sulfide.[54] Meanwhile, biotic reduction of strengite and dissolution of chemically bound phosphate were released into AD process waters.[47] Therefore, vivianite and Fe sulfides were enriched in the final AD solids. For HT hydrochars derived from higher HT temperatures (155 and 185 °C), the fraction of vivianite in the final AD solids was lower. Hydrochars mainly behave as electron shuttle,[70,71] whereas biomass available for oxidation had a lower concentration

https://dx.doi.org/10.1021/acssuschemeng.0c05544
ACS Sustainable Chem. Eng. 2020, 8, 16515−16525

during the second-stage AD, inhibiting the coupled reduction of Fe(III). For Fe sulfides, pyrite was much more stable than FeS during AD because FeS can react with hydrogen sulfide to form pyrite.[72,73] According to the S and Fe XAS LCF analyses, pyrite fraction in the final AD solids took up ~37% of the total S content but was very low as an Fe species. That is because the total concentration of Fe in the AD final solids was much higher than that of S.

Comparison of AD, HT−AD, and AD−HT−AD. On the basis of our previous[29] and present studies, the cycling of both P and S was strongly coupled with Fe chemistry. The changes in the main Fe-associated P and S fractions during various treatment systems are summarized in Figure 5. The prestage

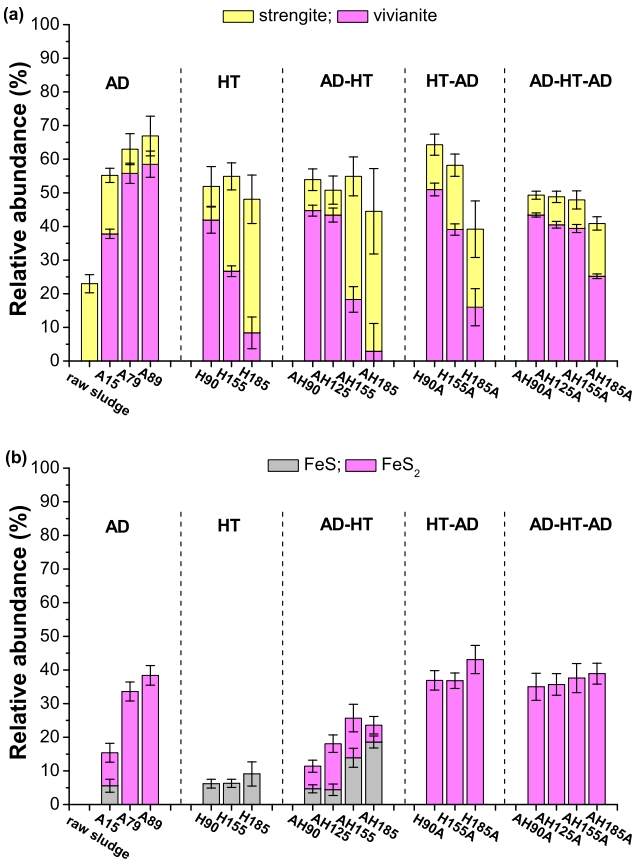

Figure 5. Summary of findings on the main Fe-associated P and S species from different treatment systems. (a) vivianite and strengite; (b) FeS and FeS_2. The same raw sludge (i.e., a blend of primary and waste activated sludge mixtures) was used for all systems. The relative abundances of vivianite, strengite, FeS, and FeS_2 were determined from the linear combination fitting (LCF) of both P and S K-edge XANES data of the solid samples. Results of A79, HT, and HT−AD are reported in Wang et al.[29] The sample labels for HT−AD are provided in Table S9.

HT at 90 °C favored vivianite formation in HT hydrochars, whereas the interstage HT at low temperatures (90 and 125 °C) did not significantly change vivianite fraction in HT hydrochars. Moreover, both pre- and interstage HTs at low temperatures (90 or 125 °C) resulted in a little more vivianite formation during the subsequent AD. Compared with AD alone, both pre- and interstage HTs at high temperatures (155 and 185 °C) inhibited the precipitation of vivianite during the subsequent AD.

When HT temperature increased from 90 to 185 °C, the fraction of FeS in the prestage HT hydrochars fluctuated between 6% and 9% of S, while the interstage HT favored the formation of FeS (i.e., increased from 5 to 19% of S) and FeS_2 (i.e., fluctuated between 5 and 14% of S). However, both the pre- and interstage HTs had weak effects on the sulfidation of Fe during the subsequent AD as compared to AD alone. Overall, we observed similar results on the main Fe-associated P and S fractions (i.e., vivianite, strengite, and Fe sulfides) in AD final solids derived from both HT−AD and AD−HT−AD systems. Considering that the AD−HT−AD system requires one more AD unit (thus a larger footprint) and is more complex to handle as compared to the HT−AD system, for nutrient recovery consideration alone, the HT−AD system might be more economical under the studied condition and scale.

We also compared the ultimate methane production of the HT−AD and AD−HT−AD systems, which refers to the highest value of methane produced from the whole treatment system (i.e., the single anaerobic reactor in the HT−AD system and the two anaerobic reactors in the AD−HT−AD system) over a long incubation time of the batch system. Below, we briefly summarize our findings (detailed results will be reported in a parallel study). Compared to AD alone (i.e., the control), in both HT−AD and AD−HT−AD systems, the overall ultimate methane production increased, and the extent of increase for each system was positively correlated with increasing HT temperature at 90−155 °C. Specifically, compared to AD alone, the increase was from 5.5 to 16.8% for the HT−AD system and from 13.7 to 29.4% for the AD−HT−AD system for HT temperature from 90 to 155 °C. However, the overall ultimate methane production was comparable for these two systems with a relative difference of 5.5−8.3% at a HT temperature of 90−155 °C. For either system, the ultimate methane production at the highest HT temperature tested (185 °C) was lower than or comparable to that at lower HT temperatures. Therefore, from the perspective of biogas production, we consider 155 °C to be the optimal HT temperature under the examined experimental setup.

This study provides fundamental knowledge for the selection and optimization of HT treatment conditions in conjunction with AD for P recovery. P from sewage sludge can be recovered via extraction of vivianite,[48] for instance, via magnetic separation from anaerobically digested sludge.[30] Our study indicates that the interstage HT at 90 and 125 °C had no apparent effect on vivianite yield during the subsequent AD, whereas higher HT temperatures (155 and 185 °C) had negative impacts on the P recovery via vivianite.

This study also has important implications for understanding the nutrient speciation and availability in anaerobically digested sludge-derived hydrochars and AD solids. For instance, when biosolids rich in vivianite are land-applied, vivianite can release P in the oxisoils and might be used as a phosphate fertilizer.[74] The organic acids (e.g., critic acid) in soils can also increase the solubility of vivianite.[75] Moreover, S speciation information during AD−HT−AD is important for understanding S bioavailability in HT hydrochars and AD solids serving as soil amendment.[76] Changes in S chemistry of biosolids strongly affect the solubility and bioavailability of toxic metals, due to thiols and sulfides for metal complexation.[77]

https://dx.doi.org/10.1021/acssuschemeng.0c05544
ACS Sustainable Chem. Eng. 2020, 8, 16515−16525

CONCLUSIONS

The speciation evolution of P, Fe, and S during the AD−HT−AD of sewage sludge was systematically studied using combined sequential chemical extraction, bulk XAS, XRD, and SEM-EDX analyses. The main results are as follows: (1) Vivianite was the predominant species of Fe and P in the anaerobically digested sewage sludge. (2) HT of anaerobically digested sludge at low temperatures (90 and 125 °C) weakly affected the speciation transformation of P, Fe, and S. However, HT at high temperatures (155 and 185 °C) induced partial auto-oxidation of vivianite into strengite and favored the production of FeS. (3) AD of HT slurries reduced strengite to vivianite and favored the transformation of FeS into pyrite. (4) Compared with AD alone (over 70 d), both HT−AD and AD−HT−AD systems at high HT temperatures (155 and 185 °C) inhibited the production of vivianite in the final AD solids, while the inhibition effects at low HT temperatures (90 and 125 °C) were much weaker. Both the HT−AD and AD−HT−AD systems did not generate more Fe sulfides in the final AD solids as compared to AD alone (over 70 d). Compared with HT−AD, AD−HT−AD yielded similar speciation of Fe, P, and S in the final AD solids. Thus, the evolution of vivianite and iron sulfides in sewage sludge depends on the treatment techniques/conditions, which need to be considered for the selection and development of appropriate nutrient reclamation/recycling methods.

ASSOCIATED CONTENT

Supporting Information

The Supporting Information is available free of charge at https://pubs.acs.org/doi/10.1021/acssuschemeng.0c05544.

Text for SCE, XAS, XRD, and SEM-EDX analyses; P fractionation by SCE analysis; reference compounds used for XAS LCF analyses; results of the major elemental concentrations in the solids and process waters; results of Fe and P K-edge XANES analysis; Fe, P, and S LCF results; and SEM-EDX data (PDF)

AUTHOR INFORMATION

Corresponding Author

Yuanzhi Tang − *School of Earth and Atmospheric Sciences and School of Civil and Environmental Engineering, Georgia Institute of Technology, Atlanta, Georgia 30332-0340, United States;* orcid.org/0000-0002-7741-8646; Phone: (1) 404-894-3814; Email: yuanzhi.tang@eas.gatech.edu

Authors

Qian Wang − *School of Earth and Atmospheric Sciences, Georgia Institute of Technology, Atlanta, Georgia 30332-0340, United States*

Chiqian Zhang − *School of Civil and Environmental Engineering, Georgia Institute of Technology, Atlanta, Georgia 30332-0512, United States;* orcid.org/0000-0003-4532-7376

Pan Liu − *School of Earth and Atmospheric Sciences, Georgia Institute of Technology, Atlanta, Georgia 30332-0340, United States*

Haesung Jung − *School of Earth and Atmospheric Sciences, Georgia Institute of Technology, Atlanta, Georgia 30332-0340, United States;* orcid.org/0000-0002-8795-248X

Biao Wan − *School of Earth and Atmospheric Sciences, Georgia Institute of Technology, Atlanta, Georgia 30332-0340, United States*

Dhara Patel − *School of Earth and Atmospheric Sciences, Georgia Institute of Technology, Atlanta, Georgia 30332-0340, United States*

Spyros G. Pavlostathis − *School of Civil and Environmental Engineering, Georgia Institute of Technology, Atlanta, Georgia 30332-0512, United States;* orcid.org/0000-0001-9731-3836

Complete contact information is available at: https://pubs.acs.org/10.1021/acssuschemeng.0c05544

Notes

The authors declare no competing financial interest.

ACKNOWLEDGMENTS

This study was supported by the U.S. National Science Foundation under Grant No. 1739884 (Y.T.). We acknowledge beamline scientists at BL 4-1 and BL 14-3 at the Stanford Synchrotron Radiation Lightsource (SSRL) for technical assistance on data collection. A portion of this research was conducted at SSRL, a U.S. Department of Energy (DOE) Office of Science User Facility operated for the DOE Office of Science by SLAC National Accelerator Laboratory under Contract No. DE-AC02-76SF00515.

REFERENCES

(1) Seiple, T. E.; Coleman, A. M.; Skaggs, R. L. Municipal wastewater sludge as a sustainable bioresource in the United States. *J. Environ. Manag.* **2017**, *197*, 673−680.

(2) Qian, L.; Wang, S.; Xu, D.; Guo, Y.; Tang, X.; Wang, L. Treatment of municipal sewage sludge in supercritical water: A review. *Water Res.* **2016**, *89*, 118−131.

(3) Caccavo, F.; Frolund, B.; Van Ommen, K. F.; Nielsen, P. H. Deflocculation of activated sludge by the dissimilatory Fe(III)-reducing bacterium *Shewanella alga* BrY. *Appl. Environ. Microbiol.* **1996**, *62*, 1487−1490.

(4) Westerhoff, P.; Lee, S.; Yang, Y.; Gordon, G. W.; Hristovski, K.; Halden, R. U.; Herckes, P. Characterization, recovery opportunities, and valuation of metals in municipal sludges from U.S. wastewater treatment plants nationwide. *Environ. Sci. Technol.* **2015**, *49*, 9479−9488.

(5) Xie, M.; Nghiem, L. D.; Price, W. E.; Elimelech, M. Toward resource recovery from wastewater: extraction of phosphorus from digested sludge using a hybrid forward osmosis−membrane distillation process. *Environ. Sci. Technol. Lett.* **2014**, *1*, 191−195.

(6) Peccia, J.; Westerhoff, P. We should expect more out of our sewage sludge. *Environ. Sci. Technol.* **2015**, *49*, 8271−8276.

(7) Carballa, M.; Duran, C.; Hospido, A. Should we pretreat solid waste prior to anaerobic digestion? An assessment of its environmental cost. *Environ. Sci. Technol.* **2011**, *45*, 10306−10314.

(8) Withers, P. J. A.; Elser, J. J.; Hilton, J.; Ohtake, H.; Schipper, W. J.; van Dijk, K. C. Greening the global phosphorus cycle: how green chemistry can help achieve planetary P sustainability. *Green Chem.* **2015**, *17*, 2087−2099.

(9) Vogel, C.; Radtke, M.; Reinholz, U.; Schäfers, F.; Adam, C. Chemical state of chromium, sulfur, and iron in sewage sludge ash based phosphorus fertilizers. *ACS Sustainable Chem. Eng.* **2015**, *3*, 2376−2380.

(10) Pavlostathis, S. G. Kinetics and modeling of anaerobic treatment and biotransformation processes. *Compr. Biotechnol.* **2011**, *6*, 385−397.

(11) Battistoni, P.; Pavan, P.; Prisciandaro, M.; Cecchi, F. Struvite crystallization: a feasible and reliable way to fix phosphorus in anaerobic supernatants. *Water Res.* **2000**, *34*, 3033−3041.

(12) Wilfert, P.; Dugulan, A. I.; Goubitz, K.; Korving, L.; Witkamp, G. J.; Van Loosdrecht, M. C. M. Vivianite as the main phosphate mineral in digested sewage sludge and its role for phosphate recovery. *Water Res.* **2018**, *144*, 312−321.
(13) Wilfert, P.; Mandalidis, A.; Dugulan, A. I.; Goubitz, K.; Korving, L.; Temmink, H.; Witkamp, G. J.; Van Loosdrecht, M. C. M. Vivianite as an important iron phosphate precipitate in sewage treatment plants. *Water Res.* **2016**, *104*, 449−460.
(14) Wilfert, P.; Kumar, P. S.; Korving, L.; Witkamp, G.-J.; van Loosdrecht, M. C. M. The relevance of phosphorus and iron chemistry to the recovery of phosphorus from wastewater: A review. *Environ. Sci. Technol.* **2015**, *49*, 9400−9414.
(15) Wu, Y.; Luo, J.; Zhang, Q.; Aleem, M.; Fang, F.; Xue, Z.; Cao, J. Potentials and challenges of phosphorus recovery as vivianite from wastewater: A review. *Chemosphere* **2019**, *226*, 246−258.
(16) Roussel, J.; Carliell-Marquet, C. Significance of vivianite precipitation on the mobility of iron in anaerobically digested sludge. *Front. Environ. Sci.* **2016**, *4*, No. 00060.
(17) Takashima, M.; Tanaka, Y. Acidic thermal post-treatment for enhancing anaerobic digestion of sewage sludge. *J. Environ. Chem. Eng.* **2014**, *2*, 773−779.
(18) Vavilin, V. A.; Fernandez, B.; Palatsi, J.; Flotats, X. Hydrolysis kinetics in anaerobic degradation of particulate organic material: An overview. *Waste Manage.* **2008**, *28*, 939−951.
(19) Ariunbaatar, J.; Panico, A.; Esposito, G.; Pirozzi, F.; Lens, P. N. Pretreatment methods to enhance anaerobic digestion of organic solid waste. *Appl. Energy* **2014**, *123*, 143−156.
(20) Nielsen, H. B.; Thygesen, A.; Thomsen, A. B.; Schmidt, J. E. Anaerobic digestion of waste activated sludge-comparison of thermal pretreatments with thermal inter-stage treatments. *J. Chem. Technol. Biotechnol.* **2011**, *86*, 238−245.
(21) Ortega-Martinez, E.; Sapkaite, I.; Fdz-Polanco, F.; Donoso-Bravo, A. From pre-treatment toward inter-treatment. Getting some clues from sewage sludge biomethanation. *Bioresour. Technol.* **2016**, *212*, 227−235.
(22) Passos, F.; Ferrer, I. Influence of hydrothermal pretreatment on microalgal biomass anaerobic digestion and bioenergy production. *Water Res.* **2015**, *68*, 364−373.
(23) Barber, W. P. F. Thermal hydrolysis for sewage treatment: A critical review. *Water Res.* **2016**, *104*, 53−71.
(24) Hii, K.; Baroutian, S.; Parthasarathy, R.; Gapes, D. J.; Eshtiaghi, N. A review of wet air oxidation and thermal hydrolysis technologies in sludge treatment. *Bioresour. Technol.* **2014**, *155*, 289−299.
(25) Takashima, M. Examination on process configurations incorporating thermal treatment for anaerobic digestion of sewage sludge. *J. Environ. Eng.* **2008**, *134*, 543−549.
(26) Fang, C.; Huang, R.; Dykstra, C.; Jiang, R.; Pavlostathis, S. G.; Tang, Y. Energy and nutrient recovery from sewage sludge and manure via anaerobic digestion with hydrothermal pretreatment. *Environ. Sci. Technol.* **2020**, *54*, 1147−1156.
(27) Christodoulou, A.; Stamatelatou, K. Overview of legislation on sewage sludge management in developed countries worldwide. *Water Sci. Technol.* **2015**, *73*, 453−462.
(28) Peccia, J.; Paez-Rubio, T. *Quantification of airborne biological contaminants associated with land-applied biosolids*; Water Environment Research Foundation:Alexandria, VA, 2007.
(29) Wang, Q.; Zhang, C.; Patel, D.; Jung, H.; Liu, P.; Wan, B.; Pavlostathis, S. G.; Tang, Y. Coevolution of iron, phosphorus, and sulfur speciation during anaerobic digestion with hydrothermal pretreatment of sewage sludge. *Environ. Sci. Technol.* **2020**, *54*, 8362−8372.
(30) Prot, T.; Nguyen, V. H.; Wilfert, P.; Dugulan, A. I.; Goubitz, K.; De Ridder, D. J.; Korving, L.; Rem, P.; Bouderbala, A.; Witkamp, G. J.; van Loosdrecht, M. C. M. Magnetic separation and characterization of vivianite from digested sewage sludge. *Sep. Purif. Technol.* **2019**, *224*, 564−579.
(31) Bostick, B. C.; Fendorf, S. Arsenite sorption on troilite (FeS) and pyrite (FeS_2). *Geochim. Cosmochim. Acta* **2003**, *67*, 909−921.
(32) Bower, J.; Savage, K. S.; Weinman, B.; Barnett, M. O.; Hamilton, W. P.; Harper, W. F. Immobilization of mercury by pyrite (FeS_2). *Environ. Pollut.* **2008**, *156*, 504−514.
(33) Gong, Y.; Tang, J.; Zhao, D. Application of iron sulfide particles for groundwater and soil remediation: A review. *Water Res.* **2016**, *89*, 309−320.
(34) Wilson, C. A.; Novak, J. T. Hydrolysis of macromolecular components of primary and secondary wastewater sludge by thermal hydrolytic pretreatment. *Water Res.* **2009**, *43*, 4489−4498.
(35) Hansel, C. M.; Benner, S. G.; Neiss, J.; Dohnalkova, A.; Kukkadapu, R. K.; Fendorf, S. Secondary mineralization pathways induced by dissimilatory iron reduction of ferrihydrite under advective flow. *Geochim. Cosmochim. Acta* **2003**, *67*, 2977−2992.
(36) Wu, H.; Ikeda-Ohno, A.; Wang, Y.; Waite, T. D. Iron and phosphorus speciation in Fe-conditioned membrane bioreactor activated sludge. *Water Res.* **2015**, *76*, 213−226.
(37) Wu, H.; Wang, Y.; Ikeda-Ohno, A.; Miller, C. J.; Waite, T. D. Impact of ferrous iron dosing on iron and phosphorus solids speciation and transformation in a pilot scale membrane bioreactor. *Environ. Sci.: Water Res. Technol.* **2019**, *5*, 1400−1411.
(38) Chen, C.; Dynes, J. J.; Wang, J.; Sparks, D. L. Properties of Fe-organic matter associations via coprecipitation versus adsorption. *Environ. Sci. Technol.* **2014**, *48*, 13751−13759.
(39) Sandström, M.; Jalilehvand, F.; Damian, E.; Fors, Y.; Gelius, U.; Jones, M.; Salomé, M. Sulfur accumulation in the timbers of King Henry VIII's warship *Mary Rose*: a pathway in the sulfur cycle of conservation concern. *Proc. Natl. Acad. Sci. U.S.A.* **2005**, *102*, 14165−14170.
(40) Bohic, S.; Murphy, K.; Paulus, W.; Cloetens, P.; Salomé, M.; Susini, J.; Double, K. Intracellular chemical imaging of the developmental phases of human neuromelanin using synchrotron X-ray microspectroscopy. *Anal. Chem.* **2008**, *80*, 9557−9566.
(41) Prietzel, J.; Botzaki, A.; Tyufekchieva, N.; Brettholle, M.; Thieme, J.; Klysubun, W. Sulfur speciation in soil by S K-edge XANES spectroscopy: comparison of spectral deconvolution and linear combination fitting. *Environ. Sci. Technol.* **2011**, *45*, 2878−2886.
(42) Cuif, J.-P.; Dauphin, Y.; Doucet, J.; Salome, M.; Susini, J. XANES mapping of organic sulfate in three scleractinian coral skeletons. *Geochim. Cosmochim. Acta* **2003**, *67*, 75−83.
(43) Latif, M. A.; Mehta, C. M.; Batstone, D. J. Low pH anaerobic digestion of waste activated sludge for enhanced phosphorous release. *Water Res.* **2015**, *81*, 288−293.
(44) Vardanyan, A.; Kafa, N.; Konstantinidis, V.; Shin, S. G.; Vyrides, I. Phosphorus dissolution from dewatered anaerobic sludge: Effect of pHs, microorganisms, and sequential extraction. *Bioresour. Technol.* **2018**, *249*, 464−472.
(45) Nielsen, P. H.; McIlroy, S. J.; Albertsen, M.; Nierychlo, M. Re-evaluating the microbiology of the enhanced biological phosphorus removal process. *Curr. Opin. Biotechnol.* **2019**, *57*, 111−118.
(46) Li, W.; Joshi, S. R.; Hou, G.; Burdige, D. J.; Sparks, D. L.; Jaisi, D. P. Characterizing phosphorus speciation of Chesapeake Bay sediments using chemical extraction, ^{31}P NMR, and X-ray absorption fine structure spectroscopy. *Environ. Sci. Technol.* **2015**, *49*, 203−211.
(47) Rasmussen, H.; Nielsen, P. H. Iron reduction in activated sludge measured with different extraction techniques. *Water Res.* **1996**, *30*, 551−558.
(48) Prot, T.; Wijdeveld, W.; Eshun, L. E.; Dugulan, A. I.; Goubitz, K.; Korving, L.; Van Loosdrecht, M. C. M. Full-scale increased iron dosage to stimulate the formation of vivianite and its recovery from digested sewage sludge. *Water Res.* **2020**, *182*, No. 115911.
(49) Seitz, M. A.; Riedner, R. J.; Malhotra, S. K.; Kipp, R. J. Iron-phosphate compound identification in sewage sludge residue. *Environ. Sci. Technol.* **1973**, *7*, 354−357.
(50) Rothe, M.; Kleeberg, A.; Hupfer, M. The occurrence, identification and environmental relevance of vivianite in waterlogged soils and aquatic sediments. *Earth Sci. Rev.* **2016**, *158*, 51−64.
(51) Frossard, E.; Bauer, J. P.; Lothe, F. Evidence of vivianite in $FeSO_4$-flocculated sludges. *Water Res.* **1997**, *31*, 2449−2454.

https://dx.doi.org/10.1021/acssuschemeng.0c05544
ACS Sustainable Chem. Eng. 2020, 8, 16515−16525

(52) Flores-Alsina, X.; Solon, K.; Kazadi Mbamba, C.; Tait, S.; Gernaey, K. V.; Jeppsson, U.; Batstone, D. J. Modelling phosphorus (P), sulfur (S) and iron (Fe) interactions for dynamic simulations of anaerobic digestion processes. *Water Res.* **2016**, *95*, 370−382.
(53) Van Hullebusch, E.; Rossano, S.; Farges, F.; Lenz, M.; Labanowski, J.; Lagarde, P.; Flank, A.; Lens, P. Sulfur K-edge XANES spectroscopy as a tool for understanding sulfur chemical state in anaerobic granular sludge. *J. Phys.: Conf. Ser.* **2009**, *190*, No. 012184.
(54) Yan, L.; Ye, J.; Zhang, P.; Xu, D.; Wu, Y.; Liu, J.; Zhang, H.; Fang, W.; Wang, B.; Zeng, G. Hydrogen sulfide formation control and microbial competition in batch anaerobic digestion of slaughterhouse wastewater sludge: Effect of initial sludge pH. *Biores. Technol.* **2018**, *259*, 67−74.
(55) Lehtoranta, J.; Ekholm, P.; Pitkänen, H. Coastal eutrophication thresholds: a matter of sediment microbial processes. *AMBIO* **2009**, *38*, 303−308.
(56) Li, R.; Cui, J.; Li, X.; Li, X. Phosphorus removal and recovery from wastewater using Fe-dosing bioreactor and cofermentation: investigation by X-ray absorption near-edge structure spectroscopy. *Environ. Sci. Technol.* **2018**, *52*, 14119−14128.
(57) Wild, D.; Kisliakova, A.; Siegrist, H. Prediction of recycle phosphorus loads from anaerobic digestion. *Water Res.* **1997**, *31*, 2300−2308.
(58) Haaning Nielsen, A.; Lens, P.; Vollertsen, J.; Hvitved-Jacobsen, T. Sulfide−iron interactions in domestic wastewater from a gravity sewer. *Water Res.* **2005**, *39*, 2747−2755.
(59) Huang, R.; Zhang, B.; Saad, E. M.; Ingall, E. D.; Tang, Y. Speciation evolution of zinc and copper during pyrolysis and hydrothermal carbonization treatments of sewage sludges. *Water Res.* **2018**, *132*, 260−269.
(60) Ghanim, B. M.; Kwapinski, W.; Leahy, J. J. Speciation of nutrients in hydrochar produced from hydrothermal carbonization of poultry litter under different treatment conditions. *ACS Sustainable Chem. Eng.* **2018**, *6*, 11265−11272.
(61) Appels, L.; Degrève, J.; Van der Bruggen, B.; Van Impe, J.; Dewil, R. Influence of low temperature thermal pre-treatment on sludge solubilisation, heavy metal release and anaerobic digestion. *Bioresour. Technol.* **2010**, *101*, 5743−5748.
(62) Tien, P.-l.; Waugh, T. C. Thermal and X-ray studies on earthy vivianite in Graneros Shale (Upper Cretaceous), Kansas. *Am. Mineral.* **1969**, *54*, 1355−1362.
(63) Hanzel, D.; Meisel, W.; Hanzel, D.; Gütlich, P. Mössbauer effect study of the oxidation of vivianite. *Solid State Commun.* **1990**, *76*, 307−310.
(64) McCammon, C. A.; Burns, R. G. The oxidation mechanism of vivianite as studies by Möessbauer spectroscopy. *Am. Mineral.* **1980**, *65*, 361−366.
(65) Pratt, A. R. Vivianite auto-oxidation. *Phys. Chem. Miner.* **1997**, *25*, 24−27.
(66) Liang, Y.; Chai, L.; Min, X.; Tang, C.; Zhang, H.; Ke, Y.; Xie, X. Hydrothermal sulfidation and floatation treatment of heavy-metal-containing sludge for recovery and stabilization. *J. Hazard. Mater.* **2012**, *217-218*, 307−314.
(67) Zhang, J.; Zuo, W.; Tian, Y.; Chen, L.; Yin, L.; Zhang, J. Sulfur transformation during microwave and conventional pyrolysis of sewage sludge. *Environ. Sci. Technol.* **2017**, *51*, 709−717.
(68) Dewil, R.; Baeyens, J.; Roels, J.; Van De Steene, B. Distribution of sulphur compounds in sewage sludge treatment. *Environ. Eng. Sci.* **2008**, *25*, 879−886.
(69) Achinas, S.; Li, Y.; Achinas, V.; Euverink, G. J. W. Biogas potential from the anaerobic digestion of potato peels: Process performance and kinetics evaluation. *Energies* **2019**, *12*, 2311−2326.
(70) Ren, S.; Usman, M.; Tsang, D. C. W.; O-Thong, S.; Angelidaki, I.; Zhu, X.; Zhang, S.; Luo, G. Hydrochar-facilitated anaerobic digestion: evidence for direct interspecies electron transfer mediated through surface oxygen-containing functional groups. *Environ. Sci. Technol.* **2020**, *54*, 5755−5766.
(71) Kappler, A.; Wuestner, M. L.; Ruecker, A.; Harter, J.; Halama, M.; Behrens, S. Biochar as an electron shuttle between bacteria and Fe(III) minerals. *Environ. Sci. Technol. Lett.* **2014**, *1*, 339−344.
(72) Wilkin, R. T.; Barnes, H. L. Pyrite formation by reactions of iron monosulfides with dissolved inorganic and organic sulfur species. *Geochim. Cosmochim. Acta* **1996**, *60*, 4167−4179.
(73) Li, Y.; van Santen, R. A.; Weber, T. High-temperature FeS−FeS_2 solid-state transitions: Reactions of solid mackinawite with gaseous H_2S. *J. Solid State Chem.* **2008**, *181*, 3151−3162.
(74) Fodoué, Y.; Nguetnkam, J.; Tchameni, R.; Basga, S.; Penaye, J. Assessment of the fertilizing effect of vivianite on the growth and yield of the bean 'Phaseolus vulgaris' on oxisoils from Ngaoundere (central north Cameroon). *Int. Res. J. Earth Sci.* **2015**, *3*, 18−26.
(75) Schütze, E.; Gypser, S.; Freese, D. Kinetics of phosphorus release from vivianite, hydroxyapatite, and bone char influenced by organic and inorganic compounds. *Soil Syst.* **2020**, *4*, 15−34.
(76) Cheah, S.; Malone, S. C.; Feik, C. J. Speciation of sulfur in biochar produced from pyrolysis and gasification of oak and corn stover. *Environ. Sci. Technol.* **2014**, *48*, 8474−8480.
(77) Prietzel, J.; Thieme, J.; Neuhäusler, U.; Susini, J.; Kögel-Knabner, I. Speciation of sulphur in soils and soil particles by X-ray spectromicroscopy. *Eur. J. Soil Sci.* **2003**, *54*, 423−433.

https://dx.doi.org/10.1021/acssuschemeng.0c05544
ACS Sustainable Chem. Eng. 2020, 8, 16515−16525